
Searching to Exploit Memorization Effect in Learning with Noisy Labels

Quanming Yao¹ Hansi Yang² Bo Han^{3,4} Gang Niu⁴ James T. Kwok⁵

Abstract

Sample selection approaches are popular in robust learning from noisy labels. However, how to properly control the selection process so that deep networks can benefit from the memorization effect is a hard problem. In this paper, motivated by the success of automated machine learning (AutoML), we model this issue as a function approximation problem. Specifically, we design a domain-specific search space based on general patterns of the memorization effect and propose a novel Newton algorithm to solve the bi-level optimization problem efficiently. We further provide theoretical analysis of the algorithm, which ensures a good approximation to critical points. Experiments are performed on both benchmark and real-world data sets. Results demonstrate that the proposed method is much better than the state-of-the-art noisy-label-learning approaches, and also much more efficient than existing AutoML algorithms.

1. Introduction

Deep networks have enjoyed huge empirical success in a wide variety of tasks, such as image processing, speech recognition, language modeling and recommender systems (Goodfellow et al., 2016). However, this highly counts on the availability of large amounts of quality data, which may not be feasible in practice. Instead, many large data sets are collected from crowdsourcing platforms or crawled from the internet, and the obtained labels are noisy (Patrini et al., 2017). As deep networks have large learning capacities, they will eventually overfit the noisy labels, leading to poor

generalization performance (Zhang et al., 2016; Arpit et al., 2017; Jiang et al., 2018).

To reduce the negative effects of noisy labels, a number of methods have been recently proposed (Sukhbaatar et al., 2015; Reed et al., 2015; Patrini et al., 2017; Ghosh et al., 2017; Malach & Shalev-Shwartz, 2017; Liu & Tao, 2015; Cheng et al., 2020). They can be grouped into three main categories. The first one is based on estimating the label transition matrix, which captures how correct labels are flipped to the wrong ones (Sukhbaatar et al., 2015; Reed et al., 2015; Patrini et al., 2017; Ghosh et al., 2017). However, this can be fragile to heavy noise and is unable to handle a large number of labels (Han et al., 2018). The second type is based on regularization (Miyato et al., 2016; Laine & Aila, 2017; Tarvainen & Valpola, 2017). However, since deep networks are usually over-parameterized, they can still completely memorize the noisy data given sufficient training time (Zhang et al., 2016).

The third approach, which is the focus in this paper, is based on selecting (or weighting) possibly clean samples in each iteration for training (Jiang et al., 2018; Han et al., 2018; Yu et al., 2019; Wang et al., 2019). Intuitively, by making the training data less noisy, better performance can be obtained. Representative methods include the MentorNet (Jiang et al., 2018) and Co-teaching (Han et al., 2018; Yu et al., 2019). Specifically, MentorNet uses an additional network to select clean samples for training of a StudentNet. Co-teaching improves MentorNet by simultaneously maintaining two networks with identical architectures during training, and each network is updated using the small-loss samples from the other network.

In sample selection, a core issue is how many small-loss samples are to be selected in each iteration. While discarding a lot of samples can avoid training with noisy labels, dropping too many can be overly conservative and lead to lower accuracy (Han et al., 2018). Co-teaching uses the observation that deep networks usually learn easy patterns before overfitting the noisy samples (Zhang et al., 2016; Arpit et al., 2017). This *memorization effect* has been widely seen in various deep networks (Patrini et al., 2017; Ghosh et al., 2017; Han et al., 2018). Hence, during the early stage of training, Co-teaching drops very few samples as the network will not memorize the noisy data. As training

¹4Paradigm Inc (Hong Kong) ²Department of Electrical Engineering, Tsinghua University ³Department of Computer Science, Hong Kong Baptist University ⁴RIKEN Center for Advanced Intelligence Project ⁵Department of Computer Science and Engineering, Hong Kong University of Science and Technology. Correspondence to: Quanming Yao <yaoquanming@4paradigm.com>.

proceeds, the network starts to memorize the noisy data. This is avoided in Co-teaching by gradually dropping more samples according to a pre-defined schedule. Empirically, this significantly improves the network’s generalization performance on noisy labels (Jiang et al., 2018; Han et al., 2018). However, it is unclear if its manually-designed schedule is “optimal”. Moreover, the schedule is not data-dependent, but is the same for all data sets. Manually finding a good schedule for each and every data set is clearly very time-consuming and infeasible.

Motivated by the recent success of automated machine learning (AutoML) (Hutter et al., 2018), in this paper we propose to exploit the memorization effect automatically using AutoML. We first formulate the learning of schedule as a bi-level optimization problem, similar to that in neural architecture search (NAS) (Zoph & Le, 2017). A search space for the schedule is designed based on the learning curve behaviors shared by deep networks. This space is expressive, and yet compact with only a small number of hyperparameters. However, computing the gradient is difficult as sample selection is a discrete operator. To avoid this problem and perform efficient search, we propose to use stochastic relaxation (Geman & Geman, 1984) together with Newton’s method to capture information from both the model and optimization objective. Convergence analysis is provided, and extensive experiments are performed on data with both synthetic and real label noise. Empirically, the proposed method outperforms state-of-the-art methods, and can select a higher proportion of clean samples than other sample selection methods. Ablation studies show that the chosen search space is appropriate, and the proposed search algorithm is faster than popular AutoML search algorithms in this context.

Notation. In the sequel, scalars are in lowercase letters, vectors are in lowercase boldface letters, and matrices are in uppercase boldface letters. The gradient of a function \mathcal{J} is denoted $\nabla \mathcal{J}$, and $\|\cdot\|$ denotes the ℓ_2 -norm of a vector.

2. Related work

2.1. Automated Machine Learning (AutoML)

Recently, AutoML has shown to be very useful in the design of machine learning models (Hutter et al., 2018; Yao & Wang, 2018). Two of its important ingredients are:

1. *Search space*, which needs to be specially designed for each AutoML problem (Baker et al., 2017; Liu et al., 2019). It should be general (so as to cover existing models), yet not too general (otherwise searching in this space will be expensive).
2. *Search algorithms*: Two types are popularly used. The first includes derivative-free optimization methods, such as reinforcement learning (Zoph & Le, 2017; Baker et al.,

2017), genetic programming (Xie & Yuille, 2017), and Bayesian optimization (Bergstra et al., 2011; Snoek et al., 2012). The second type is gradient-based, and updates the parameters and hyperparameters in an alternating manner. On NAS problems, gradient-based methods are usually more efficient than derivative-free methods (Liu et al., 2019; Akimoto et al., 2019; Yao et al., 2020).

2.2. Learning from Noisy Labels

The state-of-the-arts usually combat noisy labels by sample selection (Jiang et al., 2018; Han et al., 2018; Malach & Shalev-Shwartz, 2017; Yu et al., 2019; Wang et al., 2019), which only uses the “clean” samples (with relatively small losses) from each mini-batch for training. The general procedure is shown in Algorithm 1. Let f be the classifier to be learned. At the t th iteration, a subset $\bar{\mathcal{D}}_f$ of small-loss samples are selected from the mini-batch $\bar{\mathcal{D}}$ (step 3). These “clean” samples are then used to update the network parameters in step 4.

Algorithm 1 General procedure on using sample selection to combat noisy labels.

- 1: **for** $t = 0, \dots, T - 1$ **do**
 - 2: draw a mini-batch $\bar{\mathcal{D}}$ from \mathcal{D} ;
 - 3: select $R(t)$ small-loss samples $\bar{\mathcal{D}}_f$ from $\bar{\mathcal{D}}$ based on network’s predictions;
 - 4: update network parameter using $\bar{\mathcal{D}}_f$;
 - 5: **end for**
-

3. Proposed Method

3.1. Motivation

In step 3 of Algorithm 1, $R(\cdot)$ controls how many samples are selected into $\bar{\mathcal{D}}_f$. As can be seen from Figure 1(a), its setting is often critical to the performance, and random $R(t)$ schedules have only marginal improvements over directly training on the whole noisy data set (denoted “Baseline” in the figure) (Han et al., 2018; Ren et al., 2018). Moreover, while having a large $R(\cdot)$ can avoid training with noisy labels, dropping too many samples can lead to lower accuracy, as demonstrated in Table 8 of (Han et al., 2018).

Based on the memorization effect in deep networks (Zhang et al., 2016), Co-teaching (Han et al., 2018) (and its variant Co-teaching+ (Yu et al., 2019)) designed the following schedule:

$$R(t) = 1 - \tau \cdot \min((t/t_k)^c, 1), \quad (1)$$

where τ , c and t_k are some hyperparameters. As can be seen from Figure 1(a), it can significantly improve the performance over random schedules.

While $R(\cdot)$ is critical and that it is important to exploit

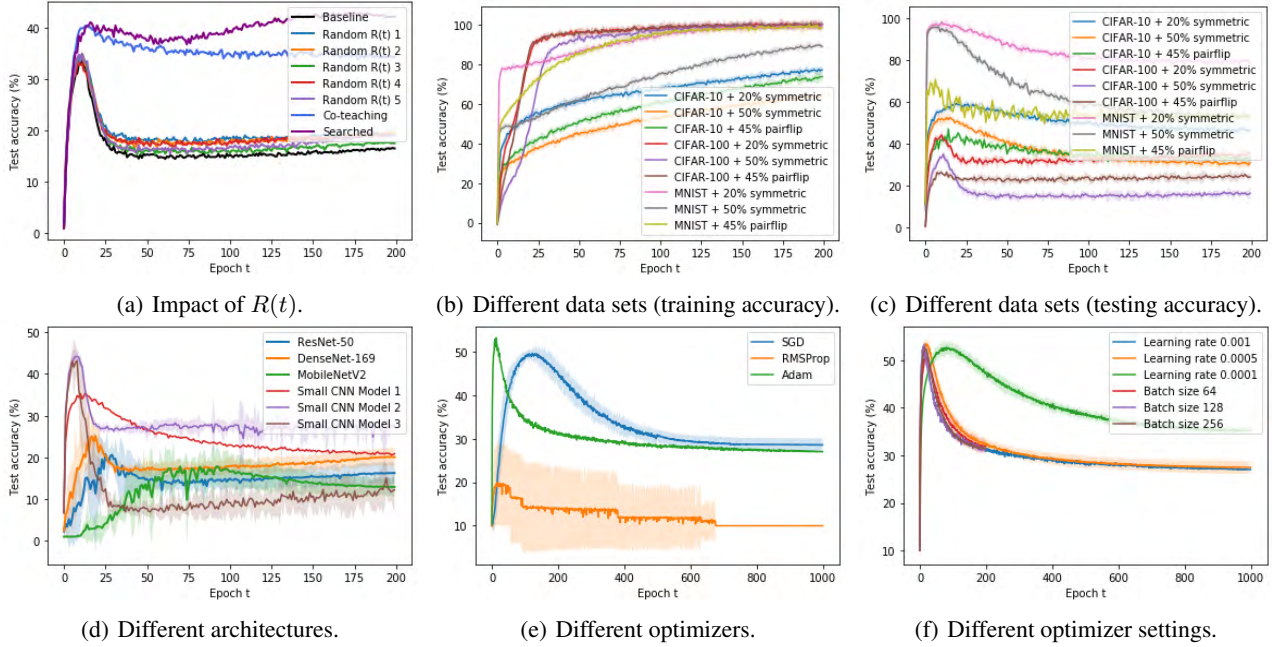


Figure 1. Training and testing accuracies on CIFAR-10, CIFAR-100, and MNIST using various architectures, optimizers, and optimizer settings. The detailed setup is in Appendix A.2.1.

the memorization effect, it is unclear if the schedule in (1) is “optimal”. Moreover, the same schedule is used by Co-teaching on all the data sets. This is expected to be suboptimal, but it is hard to find $R(\cdot)$ for each and every data set manually. This motivates us to formulate the design of $R(\cdot)$ as an AutoML problem that searches for a good $R(\cdot)$ automatically (Section 3.2). The two important ingredients of AutoML, namely, search space and search algorithm, will then be described in Sections 3.3 and 3.4, respectively.

3.2. Formulation as an AutoML Problem

Let the noisy training (resp. clean validation) data set be \mathcal{D}_{tr} (resp. \mathcal{D}_{val}), the training (resp. validation) loss be \mathcal{L}_{tr} (resp. \mathcal{L}_{val}), and f be a neural network with model parameter w . We formulate the design of $R(\cdot)$ in Algorithm 1 as the following AutoML problem:

$$R^* = \arg \min_{R(\cdot) \in \mathcal{F}} \mathcal{L}_{\text{val}}(f(w^*; R), \mathcal{D}_{\text{val}}), \quad (2)$$

$$\text{s.t. } w^* = \arg \min_w \mathcal{L}_{\text{tr}}(f(w; R), \mathcal{D}_{\text{tr}}). \quad (3)$$

where \mathcal{F} is the search space of $R(\cdot)$.

Similar to the AutoML problems of auto-sklearn (Feurer et al., 2015) and NAS (Zoph & Le, 2017; Liu et al., 2019; Yao et al., 2020), this is also a bi-level optimization problem (Colson et al., 2007). At the outer level (subproblem (2)), a good $R(\cdot)$ is searched based on the validation set. At the lower level (subproblem (3)), we find the model parameters using the training set.

3.3. Designing the Search Space \mathcal{F}

In Section 3.3.1, we first discuss some observations from the learning curves of deep networks. These are then used in the design of an appropriate search space for $R(\cdot)$ in Section 3.3.2.

3.3.1. OBSERVATIONS FROM LEARNING CURVES

Figures 1(b)-1(f) show the training and validation set accuracies obtained on the MNIST, CIFAR-10, CIFAR-100 data sets, which are corrupted with different types and levels of label noise (symmetric flipping 20%, symmetric flipping 50%, and pair flipping 45%), using a number of architectures (ResNet (He et al., 2016), DenseNet (Huang et al., 2017) and small CNN models in (Yu et al., 2019)), optimizers (SGD (Bottou, 2010), Adam (Kingma & Ba, 2014) and RMSProp (Hinton et al., 2012)) and optimizer settings (learning rate and batch size).

As can be seen, the training accuracy always increases as training progresses (Figure 1(b)), while the testing accuracy first increases and then slowly drops due to over-fitting (Figure 1(c)). Note that this pattern is independent of the network architecture (Figure 1(d)), choice of optimizer (Figure 1(e)), and hyperparameter (Figure 1(f)).

Recall that deep networks usually learn easy patterns first before memorizing and overfitting the noisy samples (Arpit et al., 2017). From (1) and Figure 1, we have the following observations on $R(t)$:

- During the initial phase when the learning curve rises, the

deep network is plastic and can learn easy patterns from the data. In this phase, one can allow a larger $R(t)$ as there is little risk of memorization. Hence, at time $t = 0$, we can set $R(0) = 1$ and the entire noisy data set is used.

- As training proceeds and the learning curve has peaked, the network starts to memorize and overfit the noisy samples. Hence, $R(t)$ should then decrease. As can be seen from Figure 1(a), this can significantly improve the network’s generalization performance on noisy labels.
- Finally, as the network gets less plastic and in case $R(t)$ drops too much at the beginning, it may be useful to allow $R(t)$ to slowly increase so as to enable learning.

The above motivates us to impose the following prior knowledge on the search space \mathcal{F} of $R(\cdot)$. An example $R(\cdot)$ is shown in Figure 2.

Assumption 1 (A Prior on \mathcal{F}). *The shape of $R(\cdot)$ should be opposite to that of the learning curve. Besides, as in (Han et al., 2018; Yu et al., 2019), it is natural to have $R(t) \in [0, 1]$ and $R(0) = 1$.*

3.3.2. IMPOSING PRIOR KNOWLEDGE

To allow efficient search, the search space has to be small but not too small. To achieve this, we impose the prior knowledge proposed in Section 3.3.1 on \mathcal{F} . Specifically, we use k basis functions (f_i ’s) whose shapes follow Assumption 1 (shown in Table 1 and Figure 2). The exact choice of these basis functions is not important. The search space for $R(\cdot)$ is then defined as:

$$\mathcal{F} \equiv \left\{ R(t) = \sum_{i=1}^k \alpha_i f_i(t; \beta_i) : \sum_i \alpha_i = 1, \alpha_i \geq 0 \right\}, \quad (4)$$

where β_i is the hyperparameter associated with basis function f_i . In the experiments, we set all β_i ’s to be in the range $[0, 1]$. Let $\alpha = \{\alpha_i\}$, $\beta = \{\beta_i\}$ and $\mathbf{x} \equiv \{\alpha, \beta\}$. The search algorithm to be introduced will then only need to search for a small set of hyperparameters \mathbf{x} .

Table 1. The four basis functions used to define the search space in the experiments. Here, a_i ’s are the hyperparameters.

f_1	$e^{-a_2 t^{a_1}} + a_3 \left(\frac{t}{T}\right)^{a_4}$
f_2	$e^{-a_2 t^{a_1}} + a_3 \frac{\log(1+t^{a_4})}{\log(1+T^{a_4})}$
f_3	$\frac{1}{(1+a_2 t)^{a_1}} + a_3 \left(\frac{t}{T}\right)^{a_4}$
f_4	$\frac{1}{(1+a_2 t)^{a_1}} + a_3 \frac{\log(1+t^{a_4})}{\log(1+T^{a_4})}$

With \mathcal{F} in (4), the outer problem in (2) becomes

$$\{\alpha^*, \beta^*\} = \arg \min_{R(\cdot) \in \mathcal{F}} \mathcal{L}_{\text{val}}(f(\mathbf{w}^*; R), \mathcal{D}_{\text{val}}), \quad (5)$$

and the optimal R^* in (2) is $\sum_{i=1}^k \alpha_i^* f_i(t; \beta_i^*)$.

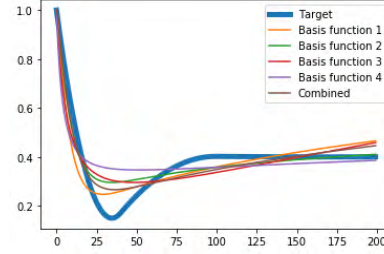


Figure 2. Plots of the basis functions in Table 1. An example $R(\cdot)$ to be learned is shown in blue.

3.3.3. DISCUSSION

As will be shown in Section 4.3.1, the search space used in Co-teaching and Co-teaching+ is not large enough to ensure good performance. Besides, the design of $R(t)$ can be considered as a function learning problem, and general function approximators (such as radial basis function networks and multilayer perceptrons) can also be used. However, as will be demonstrated in Section 4.3.1, the resultant search space is too large for efficient search, while the prior on \mathcal{F} in (4) can provide satisfactory performance. Note that the proposed search space can well approximate the space in Co-teaching (details are in Appendix B.1).

3.4. Search Algorithm Based on Relaxation

Gradient-based methods (Bengio, 2000; Liu et al., 2019; Yao et al., 2020) have been popularly used in NAS and hyperparameter optimization. Usually, the gradient w.r.t. hyperparameter \mathbf{x} is computed via the chain rule as: $\nabla_{\mathbf{x}} \mathcal{L}_{\text{val}} = \nabla_{\mathbf{w}^*} \mathcal{L}_{\text{val}} \cdot \nabla_{\mathbf{x}} \mathbf{w}^*$. However, $\nabla_{\mathbf{x}} \mathbf{w}^*$ is hard to obtain here, as the hyperparameters in $R(\cdot)$ control the selection of samples in each mini-batch, a discrete operation.

3.4.1. STOCHASTIC RELAXATION WITH NEWTON’S METHOD

To avoid a direct computation of the gradient w.r.t \mathbf{x} , we propose to transform problem (2) with stochastic relaxation (Geman & Geman, 1984). This has also been recently explored in AutoML (Baker et al., 2017; Pham et al., 2018; Akimoto et al., 2019). Specifically, instead of (2), we consider the following optimization problem:

$$\min_{\theta} \mathcal{J}(\theta) \equiv \int_{\mathbf{x} \in \mathcal{F}} \bar{f}(\mathbf{x}) p_{\theta}(\mathbf{x}) d\mathbf{x}, \quad (6)$$

where $\bar{f}(\mathbf{x}) \equiv \mathcal{L}_{\text{val}}(f(\mathbf{w}^*; R(\mathbf{x})), \mathcal{D}_{\text{val}})$ in (5), and $p_{\theta}(\mathbf{x})$ is a distribution (parametrized by θ) on the search space \mathcal{F} in (4). As $\alpha_i \geq 0$ and $\sum_i \alpha_i = 1$, we use the Dirichlet distribution on α . We use the Beta distribution on β , as each β_i lies in a bounded interval. Note that minimizing $\mathcal{J}(\theta)$ coincides with minimization of (2), i.e., $\min_{\theta} \mathcal{J}(\theta) = \min_{\mathbf{x}} \bar{f}(\mathbf{x})$ (Akimoto et al., 2019).

Let $\bar{p}_\theta(\mathbf{x}) \equiv \nabla \log p_\theta(\mathbf{x})$. As $\mathcal{J}(\theta)$ is smooth, it can be minimized by gradient descent, with

$$\nabla \mathcal{J}(\theta) = \int_{\mathbf{x} \in \mathcal{F}} \bar{f}(\mathbf{x}) \nabla p_\theta(\mathbf{x}) d\mathbf{x} = \mathbb{E}_{p_\theta} [\bar{f}(\mathbf{x}) \bar{p}_\theta(\mathbf{x})].$$

The expectation can be approximated by sampling K \mathbf{x}_i 's from $p_\theta(\cdot)$, leading to

$$\nabla \mathcal{J}(\theta) \simeq \frac{1}{K} \sum_{i=1}^K \bar{f}(\mathbf{x}_i) \bar{p}_\theta(\mathbf{x}_i). \quad (7)$$

The update at the m th iteration is then

$$\theta^{m+1} = \theta^m + \rho \mathbf{H}^{-1} \nabla \mathcal{J}(\theta^m), \quad (8)$$

where ρ is the stepsize, $\mathbf{H} = \mathbf{I}$ for gradient descent and $\mathbf{H} = \mathbb{E}_{p_\theta} [\bar{p}_\theta(\mathbf{x}) \bar{p}_\theta(\mathbf{x})^\top]$ (i.e., Fisher matrix) for natural gradient descent.

In general, natural gradient considers the geometrical structure of the underlying probability manifold, and is more efficient than simple gradient descent. However, here, the manifold is induced by a p_θ that is artificially introduced for stochastic relaxation. Subsequently, the Fisher matrix is independent of the objective \mathcal{J} . In this paper, we instead propose to use the Newton's method and set $\mathbf{H} = \nabla^2 \mathcal{J}(\theta)$, which explicitly takes \mathcal{J} into account. The following Proposition shows that the Hessian can be easily computed (proof is in Appendix C), and clearly incorporates more information than the Fisher matrix. Moreover, it can also be approximated with finite samples as in (7).

Proposition 1. $\nabla^2 \mathcal{J}(\theta) = \mathbb{E}_{p_\theta} [\bar{f}(\mathbf{x}) \nabla^2 \log p_\theta(\mathbf{x})] + \mathbb{E}_{p_\theta} [\bar{f}(\mathbf{x}) \bar{p}_\theta(\mathbf{x}) \bar{p}_\theta(\mathbf{x})^\top]$.

The whole procedure, which will be called *Search to Exploit* (S2E), is shown in Algorithm 2.

Algorithm 2 *Search to Exploit* (S2E) algorithm for the minimization of the relaxed objective \mathcal{J} in (6).

- 1: Initialize $\theta^1 = \mathbf{1}$ so that $p_\theta(\mathbf{x})$ is uniform distribution.
- 2: **for** $m = 1, \dots, M$ **do**
- 3: **for** $k = 1, \dots, K$ **do**
- 4: draw hyperparameter \mathbf{x} from distribution $p_{\theta^m}(\mathbf{x})$;
- 5: using \mathbf{x} , run Algorithm 1 with $R(\cdot)$ in (4);
- 6: **end for**
- 7: use the K samples in steps 3-6 to approximate $\nabla \mathcal{J}(\theta^m)$ in (7) and $\nabla^2 \mathcal{J}(\theta^m)$ in Proposition 1;
- 8: update θ^m by (8);
- 9: **end for**

3.4.2. CONVERGENCE ANALYSIS

When $K = \infty$ in (7), classical analysis (Rockafellar, 1970) ensures that Algorithm 2 converges at a critical point of (6). When \mathcal{J} is convex, a super-linear convergence rate is also

guaranteed. However, when $K \neq \infty$, the approximation of $\nabla \mathcal{J}(\theta)$ in (7) and the analogous approximation of $\nabla^2 \mathcal{J}(\theta)$ introduce errors into the gradient. To make this explicit, we rewrite (8) as

$$\theta^{m+1} = \theta^m - (\Delta^m)^{-1} (\nabla \mathcal{J}(\theta^m) - \mathbf{e}^m), \quad (9)$$

where Δ^m and \mathbf{e}^m are the approximated Hessian and gradient errors, respectively, at the m th iteration.

We make the following Assumption on \mathcal{J} , which requires \mathcal{J} to be smooth and bounded from below.

Assumption 2. (i) \mathcal{J} is L -Lipschitz smooth, i.e., $\|\nabla \mathcal{J}(\mathbf{x}) - \nabla \mathcal{J}(\mathbf{y})\| \leq L \|\mathbf{x} - \mathbf{y}\|$ for some positive L ; (ii) \mathcal{J} is coercive, i.e., $\inf_{\theta} \mathcal{J}(\theta) > -\infty$ and $\lim_{\|\theta\| \rightarrow \infty} \mathcal{J}(\theta) = \infty$.

We make the following Assumption 3 on (9). Note that $\bar{\epsilon} = 0$ when $K \rightarrow \infty$. However, since $K \neq \infty$ in practice, the errors in Δ^m and \mathbf{e}^m do not vanish, i.e., $\lim_{m \rightarrow \infty} [\Delta^m - \nabla^2 \mathcal{J}(\theta^m)] \neq \mathbf{0}$ and $\lim_{m \rightarrow \infty} \mathbf{e}^m \neq \mathbf{0}$, Assumption 3 is more relaxed than the typical vanishing error assumptions used in classical analysis of first-order optimization algorithms (Schmidt et al., 2011; Bolte et al., 2014; Yao et al., 2017).

Assumption 3. (i) $\eta \leq \sigma(\Delta^m) \leq L$, where $\sigma(\cdot)$ denotes eigenvalues of the matrix argument, and η is a positive constant; (ii) Gradient errors are bounded: $\forall m, \|\mathbf{e}^m\| \leq \bar{\epsilon}$.

Using Assumptions 2 and 3, the following Proposition bounds the difference in objective values at two consecutive iterations. Note that the RHS below may not be positive, and so \mathcal{J} may not be non-increasing.

Proposition 2. $\mathcal{J}(\theta^m) - \mathcal{J}(\theta^{m+1}) \geq \frac{2-L\eta}{2\eta} \|\gamma^m\|^2 - \|\mathbf{e}^m\| \|\gamma^m\|$, where $\gamma^m = \theta^{m+1} - \theta^m$.

The following Theorem shows that we can obtain an approximate critical point for which the gradient norm is bounded by a constant factor of the gradient error. As $\bar{\epsilon} = 0$ when $K \rightarrow \infty$, Theorem 1 ensures that a limit point can be obtained.

Theorem 1. Assume that $2 - L\eta + \eta^2$ and $2\eta^2 + L\eta - 2$ are non-negative. Then, (i) For every bounded sequence $\{\theta^m\}$ generated by Algorithm 2, there exists a limit point $\bar{\theta}$ such that $\|\nabla \mathcal{J}(\bar{\theta})\| \leq c_1 \bar{\epsilon}$, where c_1 is a positive constant. (ii) If $\{\theta^m\}$ converges, then $\lim_{m \rightarrow \infty} \|\mathbf{e}^m\| \leq c_2 \bar{\epsilon}$, where c_2 is a positive constant.

Proofs are in Appendix C, and are inspired by (Sra, 2012; Schmidt et al., 2011; Yao et al., 2017). However, they do not consider stochastic relaxation and the use of Hessian.

4. Experiments

In this section, we demonstrate the superiority of the proposed *Search to Exploit* (S2E) algorithm over the

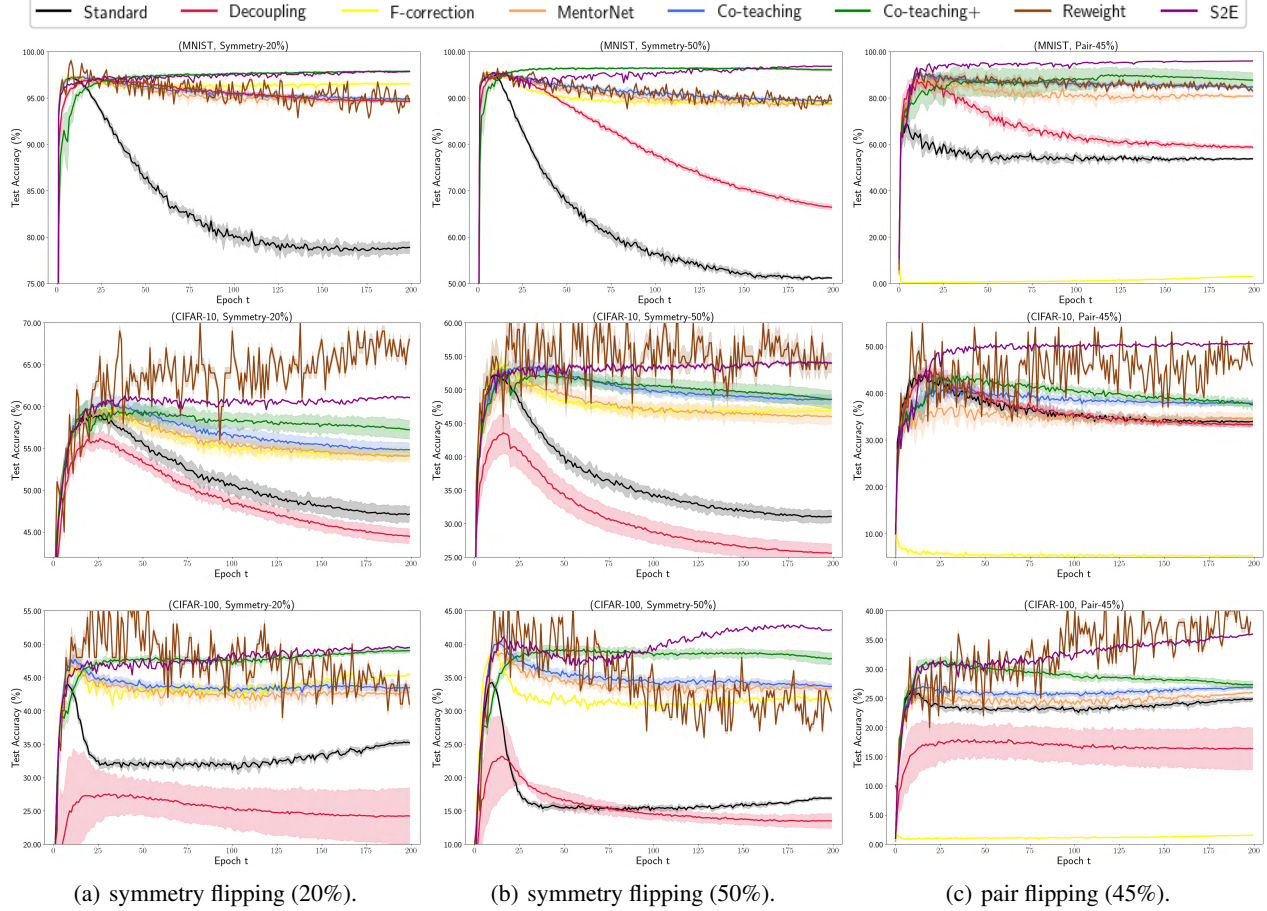


Figure 3. Testing accuracies (mean and standard deviation) on MNIST (top), CIFAR-10 (middle) and CIFAR-100 (bottom).

state-of-the-art in combating noisy labels. In step 5 of Algorithm 2, we use Co-teaching as Algorithm 1. Experiments are performed on standard benchmark data sets with artificial label noise injected (Section 4.1) and real label noise (Section 4.2). All the codes are implemented in PyTorch 0.4.1, and run on a GTX 1080 Ti GPU.

4.1. Data with Artificial Label Noise

In this experiment, we use three popular benchmark data sets: MNIST, CIFAR-10 and CIFAR-100. Following (Patrini et al., 2017; Han et al., 2018), we add two types of label noise: (i) symmetric flipping, which flips the label to other incorrect labels with equal probabilities; and (ii) pair flipping, which flips a pair of similar labels. We use the same network architectures as in (Yu et al., 2019). The detailed experimental setup is in Appendix A.1.

We compare the proposed S2E with the following state-of-the-art methods: (i) *Decoupling* (Malach & Shalev-Shwartz, 2017); (ii) *F-correction* (Patrini et al., 2017); (iii) *MentorNet* (Jiang et al., 2018); (iv) *Co-teaching* (Han et al., 2018); (v) *Co-teaching+* (Yu et al., 2019); and (vi) *Reweight* (Ren et al., 2018). As a simple baseline, we also compare with

a standard deep network (denoted *Standard*) that trains directly on the full noisy data set. All experiments are repeated five times, and we report the averaged results.

As in (Patrini et al., 2017; Han et al., 2018), Figure 3 shows convergence of the testing accuracies. As can be seen, S2E significantly outperforms the other methods and is much more stable.

4.1.1. THE $R(\cdot)$ LEARNED

Figure 4 compares the $R(\cdot)$'s obtained by the proposed S2E and the sample selection methods of *MentorNet*, *Co-teaching* and *Co-teaching+*. As can be seen, the $R(\cdot)$'s learned by S2E are dataset-specific, while the other methods always use the same $R(\cdot)$. Besides, the $R(\cdot)$ learned on the noisier data is smaller (e.g., compare symmetric-50% vs symmetric-20%). This is intuitive since a higher noise level means there are fewer clean samples (smaller $R(\cdot)$) in each mini-batch. Moreover, the proportion of large-loss samples dropped by $R(\cdot)$ is larger than the underlying noise level. Intuitively, a large-loss sample usually has a larger gradient, and can have significant impact on the model if its label is wrong. As a large-loss sample may not necessarily be noisy

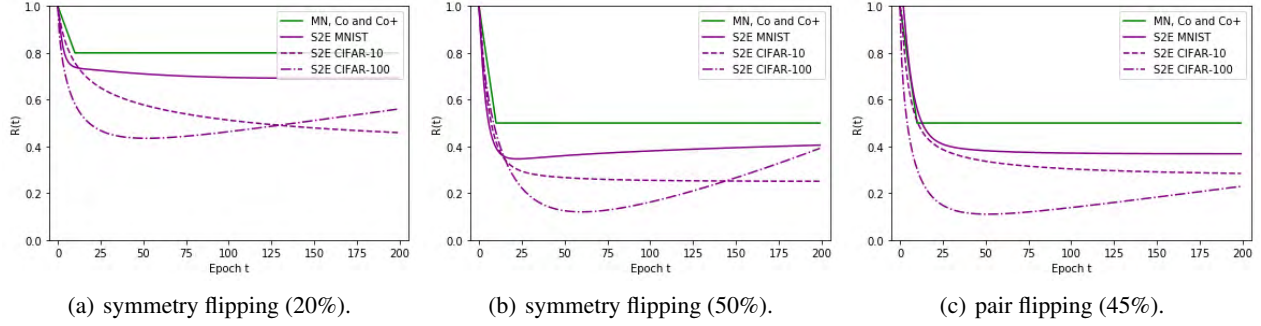


Figure 4. $R(\cdot)$ obtained by the sample selection methods. Note that *MentorNet* (MN), *Co-teaching* (Co) and *Co-teaching+* (Co+) all use the same $R(t)$.

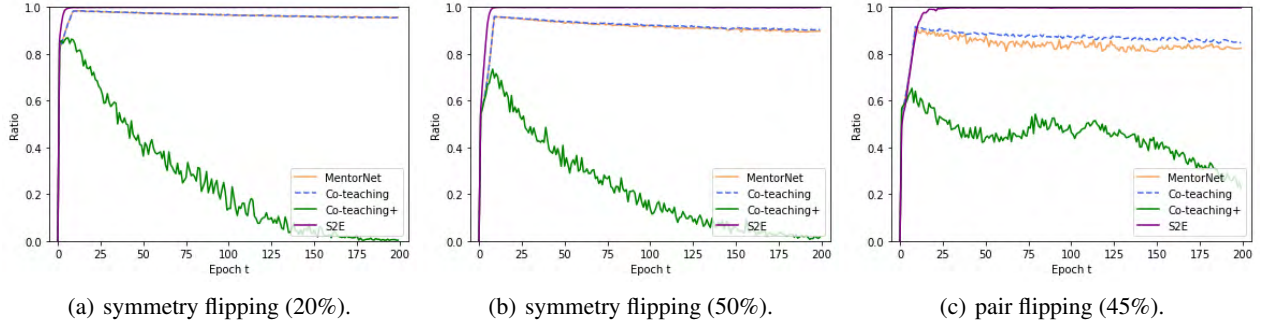


Figure 5. Label precision of *MentorNet*, *Co-teaching*, *Co-teaching+* and *S2E* on MNIST. Plots for CIFAR-10 and CIFAR-100 are in Appendix A.3.

because the model is not perfect, more samples are dropped.

On the other hand, simply dropping more samples can lead to lower accuracy (as demonstrated in Table 8 of (Han et al., 2018)). Following (Han et al., 2018), Figure 5 compares the label precision (i.e., ratio of clean samples in each mini-batch after selection) of *S2E* and other compared methods. As can be seen, *S2E*'s label precision is consistently the highest. This shows that the training samples used by *S2E* are cleaner, and thus yield better performance.

4.2. Data with Real Label Noise

In this section, we perform experiments on deep face recognition (Parkhi et al., 2015). Following (Wang et al., 2019), we use the VggFace2-R data set (Cao et al., 2018) for training, which is a noisy data set collected from Google image search. We then report the testing accuracies on four small and clean data sets: CALFW/CPLFW (Zheng & Deng, 2018), AgeDB (Moschoglou et al., 2017), and CFPW (Sengupta et al., 2016). Details of the data sets and network architectures are shown in Appendix A.1.

Besides the baselines in Section 4.1, we also compare with the state-of-the-art on this task: *Co-mining* (Wang et al., 2019), which improves *Co-teaching* by re-weighting clean samples using domain-specific information from face recognition. Table 2 shows the testing accuracies. As can be seen, *S2E* consistently outperforms the other methods.

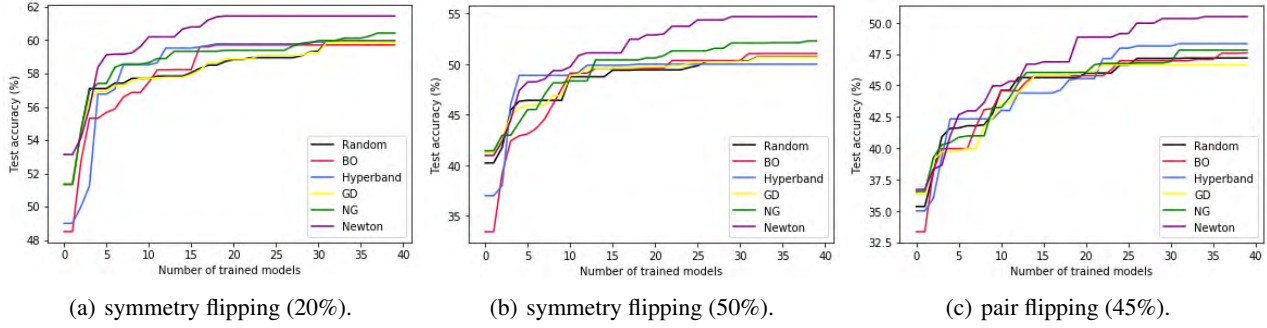
Table 2. Testing accuracies on deep face recognition. Results on the baselines are from (Wang et al., 2019). We do not compare with F-correction as its performance is not reported in (Wang et al., 2019).

	CAL-FW	CPL-FW	Age-DB	CFP-W	avg.
Standard	90.11	86.30	92.81	95.50	91.18
Decoupling	90.23	86.14	93.90	95.85	91.53
MentorNet	90.14	85.41	92.70	95.20	90.86
Co-teaching	89.90	85.05	92.05	95.05	90.62
Co-teaching+	89.43	85.23	92.50	95.41	90.64
Co-Mining	91.06	87.31	94.05	95.87	92.07
S2E	92.04	89.43	95.22	96.16	93.20

4.3. Ablation Study

4.3.1. SEARCH SPACE

In this experiment, we study different search space designs using the data sets in Section 4.1. The search space of *S2E* is compared with (i) *Co-teaching*: the space specified in (1); and (ii) *Single*: the space spanned by a single basis function in Table 1. Here, we report the best performance over the four basis functions; (iii) *RBF*: the space of functions output by a radial basis function network, with one input (epoch t), a RBF layer, and a sigmoid output unit. (iv) *MLP*: the space of functions output by a multilayer perceptron with one


 Figure 6. Search efficiency of *S2E* and the other search algorithms.

input, a single hidden layer of ReLU units, and a sigmoid output unit; The numbers of hidden units in the MLP and RBF are set to four, which is equal to the number of basis functions in *S2E*. For a fair comparison, random search is used in this experiment. This is repeated 50 times, and the average results reported.

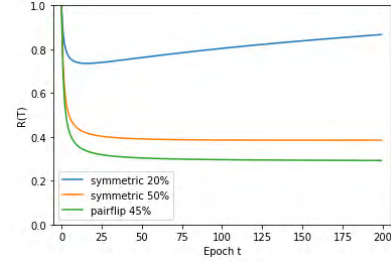
Table 3 shows the best testing accuracy over all epochs obtained by the various search space variants. *Co-teaching* and *Single* perform better than the two general function approximators (*RBF* and *MLP*), as their search spaces encapsulate the prior knowledge that $R(\cdot)$ should be of the form in Assumption 1. Figure 7 shows the $R(\cdot)$ obtained by *MLP* (which outperforms *RBF*) on the CIFAR-10 data set (results on MNIST and CIFAR-100 are similar). As can be seen, the shapes generally follow that in Assumption 1, providing further empirical evidence to support this Assumption. The performance attained by *S2E* is still the best (even though only random search is used here). This demonstrates the expressiveness and compactness of the proposed search space.

 Table 3. Best testing accuracy obtained by the various search space designs. Here, “Co” stands for *Co-teaching*, and “Sin” is *Single*.

	noise	Co	Sin	RBF	MLP	<i>S2E</i>
MNIST	sym-20%	97.83	97.67	96.94	97.69	97.87
	sym-50%	96.54	96.56	95.53	96.16	96.90
	pair-45%	93.27	94.99	89.37	93.25	95.47
CIFAR -10	sym-20%	57.24	57.83	56.58	56.82	58.73
	sym-50%	47.14	47.81	45.15	46.18	50.82
	pair-45%	44.87	45.19	42.61	44.26	47.58
CIFAR -100	sym-20%	44.89	44.93	44.24	44.57	45.32
	sym-50%	36.53	36.71	30.99	35.88	38.74
	pair-45%	27.30	31.25	27.96	28.06	32.44

4.3.2. SEARCH ALGORITHM

Recall that *S2E* uses stochastic relaxation with Newton’s method (denoted *Newton*) as the search algorithm. In this section, we study the use of other gradient-based search algorithms, including (i) gradient descent (*GD*) (Liu et al., 2019); and (ii) natural gradient descent (*NG*) (Amari, 1998);


 Figure 7. $R(t)$ obtained by *MLP* on CIFAR-10.

and also derivative-free search algorithms, including (i) random search (*random*) (Bergstra & Bengio, 2012); (ii) Bayesian optimization (*BO*) (Bergstra et al., 2011); and (iii) *hyperband* (Li et al., 2017). For fairness and consistency, all these are used with Co-teaching as in previous experiments. We do not compare with reinforcement learning (Zoph & Le, 2017), as our search problem does not involve a sequence of actions. The experiment is performed on the CIFAR-10.

In Algorithm 2, the most expensive part is step 5 where Algorithm 1 is called and model training is required. Figure 6 shows the testing accuracy w.r.t. the number of such calls. As can be seen, *S2E*, with the use of the Hessian matrix, is most efficient than the other algorithms compared.

5. Conclusion

In this paper, we address the problem of learning with noisy labels by exploiting deep networks’ memorization effect with automated machine learning (AutoML). We first design an expressive but compact search space based on observations from the learning curves. An efficient search algorithm, based on stochastic relaxation and Newton’s method, overcomes the difficulty of computing the gradient and allows incorporation of information from the model and optimization objective. Extensive experiments on both synthetic and real-world data sets demonstrate that the proposed method outperforms the state-of-the-art, and can select a higher proportion of clean samples than other sample selection methods.

Acknowledgment

This work is performed when Hansi Yang was an intern in 4Paradigm Inc supervised by Quanming Yao. Bo Han was partially supported by HKBU Tier-1 Start-up Grant and HKBU CSD Start-up Grant.

References

- Akimoto, Y., Shirakawa, S., Yoshinari, N., Uchida, K., Saito, S., and Nishida, K. Adaptive stochastic natural gradient method for one-shot neural architecture search. In *ICML*, pp. 171–180, 2019.
- Amari, S. Natural gradient works efficiently in learning. *NeuComp*, 10(2):251–276, 1998.
- Arpit, D., Jastrzbski, S., Ballas, N., Krueger, D., Bengio, E., Kanwal, M., Maharaj, T., Fischer, A., Courville, A., and Bengio, Y. A closer look at memorization in deep networks. In *ICML*, pp. 233–242, 2017.
- Baker, B., Gupta, O., Naik, N., and Raskar, R. Designing neural network architectures using reinforcement learning. In *ICLR*, 2017.
- Bengio, Y. Gradient-based optimization of hyperparameters. *NeuComp*, 12(8):1889–1900, 2000.
- Bergstra, J. and Bengio, Y. Random search for hyperparameter optimization. *JMLR*, 13(Feb):281–305, 2012.
- Bergstra, J. S., Bardenet, R., Bengio, Y., and Kégl, B. Algorithms for hyper-parameter optimization. In *NIPS*, pp. 2546–2554, 2011.
- Bolte, J., Sabach, S., and Teboulle, M. Proximal alternating linearized minimization for nonconvex and nonsmooth problems. *MathProg*, 146(1-2):459–494, 2014.
- Bottou, L. Large-scale machine learning with stochastic gradient descent. In *ICCS*, pp. 177–186, 2010.
- Cao, Q., Shen, L., Xie, W., Parkhi, O. M., and Zisserman, A. Vggface2: A dataset for recognising faces across pose and age. In *ICAFGR*, pp. 67–74, 2018.
- Cheng, J., Liu, T., Ramamohanarao, K., and Tao, D. Learning with bounded instance-and label-dependent label noise. *ICML*, 2020.
- Colson, B., Marcotte, P., and Savard, G. An overview of bilevel optimization. *Ann. Oper. Res.*, 153(1):235–256, 2007.
- Feurer, M., Klein, A., Eggenberger, K., Springenberg, J., Blum, M., and Hutter, F. Efficient and robust automated machine learning. In *NIPS*, pp. 2962–2970, 2015.
- Geman, S. and Geman, D. Stochastic relaxation, gibbs distributions, and the bayesian restoration of images. *TPAMI*, (6):721–741, 1984.
- Ghosh, A., Kumar, H., and Sastry, P. Robust loss functions under label noise for deep neural networks. In *AAAI*, pp. 1919–1925, 2017.
- Goodfellow, I., Bengio, Y., and Courville, A. *Deep Learning*. MIT, 2016.
- Han, B., Yao, Q., Yu, X., Niu, G., Xu, M., Hu, W., Tsang, I., and Sugiyama, M. Co-teaching: Robust training of deep neural networks with extremely noisy labels. In *NIPS*, pp. 8527–8537, 2018.
- He, K., Zhang, X., Ren, S., and Sun, J. Deep residual learning for image recognition. In *CVPR*, pp. 770–778, 2016.
- Hinton, G., Srivastava, N., and Swersky, K. An overview of mini-batch gradient descent. Technical report, Neural networks for machine learning: Lecture 6, 2012.
- Huang, G., Liu, Z., Van Der Maaten, L., and Weinberger, K. Q. Densely connected convolutional networks. In *CVPR*, pp. 4700–4708, 2017.
- Hutter, F., Kotthoff, L., and Vanschoren, J. (eds.). *Automated Machine Learning: Methods, Systems, Challenges*. Springer, 2018.
- Jiang, L., Zhou, Z., Leung, T., Li, J., and Li, F.-F. MentorNet: Learning data-driven curriculum for very deep neural networks on corrupted labels. In *ICML*, pp. 2309–2318, 2018.
- Kingma, D. and Ba, J. Adam: A method for stochastic optimization. In *ICLR*, 2014.
- Laine, S. and Aila, T. Temporal ensembling for semi-supervised learning. In *ICLR*, 2017.
- Li, L., Jamieson, K., DeSalvo, G., Rostamizadeh, A., and Talwalkar, A. Hyperband: A novel bandit-based approach to hyperparameter optimization. *JMLR*, 18(1):6765–6816, 2017.
- Liu, H., Simonyan, K., and Yang, Y. DARTS: Differentiable architecture search. In *ICLR*, 2019.
- Liu, T. and Tao, D. Classification with noisy labels by importance reweighting. *TPAMI*, 38(3):447–461, 2015.
- Malach, E. and Shalev-Shwartz, S. Decoupling “when to update” from “how to update”. In *NIPS*, pp. 960–970, 2017.

- Miyato, T., Maeda, S., Koyama, M., and Ishii, S. Virtual adversarial training: A regularization method for supervised and semi-supervised learning. In *ICLR*, 2016.
- Moschoglou, S., Papaioannou, A., Sagonas, C., Deng, J., Kotsia, I., and Zafeiriou, S. AgeDB: The first manually collected, in-the-wild age database. In *CVPR Workshop*, 2017.
- Parkhi, O., Vedaldi, A., and Zisserman, A. Deep face recognition. In *BMVC*, 2015.
- Patrini, G., Rozza, A., Menon, A., Nock, R., and Qu, L. Making deep neural networks robust to label noise: A loss correction approach. In *CVPR*, pp. 2233–2241, 2017.
- Pham, H., Guan, M., Zoph, B., Le, Q., and Dean, J. Efficient neural architecture search via parameter sharing. In *ICML*, pp. 4092–4101, 2018.
- Reed, S., Lee, H., Anguelov, D., Szegedy, C., Erhan, D., and Rabinovich, A. Training deep neural networks on noisy labels with bootstrapping. In *ICLR Workshop*, 2015.
- Ren, M., Zeng, W., Yang, B., and Urtasun, R. Learning to reweight examples for robust deep learning. In *ICML*, pp. 4331–4340, 2018.
- Rockafellar, R. T. *Convex Analysis*. Princeton University Press, 1970.
- Schmidt, M., Roux, N. L., and Bach, F. R. Convergence rates of inexact proximal-gradient methods for convex optimization. In *NIPS*, pp. 1458–1466, 2011.
- Sciuto, C., Yu, K., Jaggi, M., Musat, C., and Salzmann, M. Evaluating the search phase of neural architecture search. In *ICLR*, 2020.
- Sengupta, S., Chen, J. C., Castillo, C., Patel, V. M., Chellappa, R., and Jacobs, D. W. Frontal to profile face verification in the wild. In *WACV*, 2016.
- Snoek, J., Larochelle, H., and Adams, R. Practical Bayesian optimization of machine learning algorithms. In *NIPS*, pp. 2951–2959, 2012.
- Sra, S. Scalable nonconvex inexact proximal splitting. In *NIPS*, pp. 530–538, 2012.
- Sukhbaatar, S., Bruna, J., Paluri, M., Bourdev, L., and Fergus, R. Training convolutional networks with noisy labels. In *ICLR Workshop*, 2015.
- Tarvainen, A. and Valpola, H. Mean teachers are better role models: Weight-averaged consistency targets improve semi-supervised deep learning results. In *NIPS*, 2017.
- Wang, X., Wang, S., Wang, J., Shi, H., and Mei, T. Co-Mining: Deep face recognition with noisy labels. In *ICCV*, pp. 9358–9367, 2019.
- Xie, L. and Yuille, A. Genetic CNN. In *ICCV*, pp. 1388–1397, 2017.
- Yao, Q. and Wang, M. Taking human out of learning applications: A survey on automated machine learning. Technical report, Arxiv: 1810.13306, 2018.
- Yao, Q., Kwok, J., Gao, F., Chen, W., and Liu, T.-Y. Efficient inexact proximal gradient algorithm for nonconvex problems. In *IJCAI*, 2017.
- Yao, Q., Xu, J., Tu, W.-W., and Zhu, Z. Efficient neural architecture search via proximal iterations. In *AAAI*, 2020.
- Yu, X., Han, B., Yao, J., Niu, G., Tsang, I., and Sugiyama, M. How does disagreement help generalization against label corruption? In *ICML*, pp. 7164–7173, 2019.
- Zhang, C., Bengio, S., Hardt, M., Recht, B., and Vinyals, O. Understanding deep learning requires rethinking generalization. *ICLR*, 2016.
- Zheng, T. and Deng, W. Cross-pose LFW: A database for studying crosspose face recognition in unconstrained environments. Technical Report 18-01, Beijing University of Posts and Telecommunications, February 2018.
- Zoph, B. and Le, Q. Neural architecture search with reinforcement learning. In *ICLR*, 2017.

A. Experimental Details

A.1. Data Sets and Network Architectures

The MNIST, CIFAR-10, CIFAR-100 data sets are obtained from PyTorch’s torchvision package.¹ A summary is shown in Table 4. The networks (MLP on MNIST, and CNN on CIFAR-10, CIFAR-100) used are shown in Table 5. Models 1 and 2 have been used in (Yu et al., 2019) on CIFAR-10 and CIFAR-100, respectively. Model 3 has been used in (Han et al., 2018).

Table 4. Data sets with artificial label noise.

	#training	#validation	#test	#classes
MNIST	60,000	5,000	5,000	10
CIFAR-10	50,000	5,000	5,000	10
CIFAR-100	50,000	5,000	5,000	100

The VggFace2-R, CALFW, CPLFW, AgeDB, and CFPW data sets are downloaded from their corresponding websites.² A summary is shown in Table 6. We use the ResNet-50 network, and the same optimizer settings for training as in (Wang et al., 2019).

Table 6. Deep face recognition data sets (with real label noise). VggFace2-R is used for training, and CALFW /CPLFW/ AgeDB/ CFPW are used for validation and testing.

	#training	#validation	#test	#classes
VggFace2-R	3.31M	-	-	9,131
CALFW	-	6,087	6,087	5,749
CPLFW	-	5,826	5,826	5,749
AgeDB	-	8,244	8,244	568
CFPW	-	3,500	3,500	500

A.2. Details for Figure 1

A.2.1. FIGURE 1(A)

We use the CIFAR-10 dataset (Table 4), and model 1 in Table 5. The number of training epochs is 200. We use the Adam optimizer (Kingma & Ba, 2014) with momentum 0.9 and batch size 128. The initial learning rate is 0.001, and is linearly decayed to zero from the 80th epoch. The 5 random $R(T)$ s (denoted “Random R(T)” 1-5) are generated by uniform sampling the corresponding hyperparameter $x = \{\alpha, \beta\}$.

Besides the test accuracies shown in Figure 1(a), we also show in Figure 8 the random $R(T)$ s, the original $R(T)$ used

¹<https://pytorch.org/docs/stable/torchvision/datasets.html>

²The data sets are downloaded from http://www.robots.ox.ac.uk/~vgg/data/vgg_face2/, <http://www.whdeng.cn/CALFW/index.html>, <http://www.whdeng.cn/CPLFW/index.html>, <https://ibug.doc.ic.ac.uk/resources/agedb/>, and <http://www.cfpw.io>, respectively.

in Co-teaching (Han et al., 2018), the $R(T)$ obtained by $S2E$ (denoted “Searched”), and the implicit $R(T)$ corresponding to training on the whole noisy dataset (denoted “Baseline”).

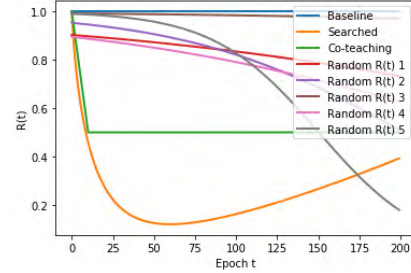


Figure 8. $R(t)$ used in Figure 1(a).

A.2.2. FIGURES 1(B)-1(C)

Experiment is performed on the MNIST/CIFAR-10/CIFAR-100 datasets (Table 4). The number of training epochs, batch size, and learning rate schedule are the same as that in Figure 1(a).

A.2.3. FIGURE 1(D)

We use the CNN models 1-3 in Table 5. As CIFAR-100 has 100 outputs, we also change the number of outputs of model 1 to 100. The number of training epochs, batch size, and learning rate schedule are the same as that in Figure 1(a).

A.2.4. FIGURE 1(E)

We use model 1 in Table 5. For Adam, the learning rate schedule is the same as that in Figure 1(a). For SGD, the initial learning rate is 0.1, and decayed to 0.01 and 0.001 at the 500th and 750th epoch, respectively. Moreover, the number of training epochs is 1000 instead of 200. For RMSProp, the learning rate is fixed at 0.01.

A.2.5. FIGURE 1(F)

The number of training epochs, batch size, and learning rate schedule are the same as that in Figure 1(a). We only change the batch size and initial learning rate as shown in the figure of Figure 1(f). Moreover, to better demonstrate the memorization effect for small learning rates, the number of training epochs is set to 1000 instead of 200.

A.3. Additional Plots for Section 4.1.1

Figure 9 compares the label precisions of the various methods on CIFAR-10 and CIFAR-100.

Table 5. MLP and CNN models used in the experiments.

MLP on MNIST	CNN on CIFAR-10 (Model 1)	CNN on CIFAR-100 (Model 2)	CNN (Model 3)
28×28 gray image	32×32 RGB image	32×32 RGB image	32×32 RGB image
Dense 28×28→256 ReLU	5×5 Conv, 6 ReLU 2×2 Max-pool	3×3 Conv, 64 BN, ReLU 3×3 Conv, 64 BN, ReLU 2×2 Max-pool	3×3 Conv, 128 BN, LReLU 3×3 Conv, 128 BN, LReLU 3×3 Conv, 128 BN, LReLU 2×2 Max-pool, stride 2 Dropout, p=0.25
	5×5 Conv, 16 ReLU 2×2 Max-pool	3×3 Conv, 128 BN, ReLU 3×3 Conv, 128 BN, ReLU 2×2 Max-pool	3×3 Conv, 256 BN, LReLU 3×3 Conv, 256 BN, LReLU 3×3 Conv, 256 BN, LReLU 2×2 Max-pool, stride 2 Dropout, p=0.25
	Dense 16×5×5→120 ReLU Dense 120→84 ReLU	3×3 Conv, 196 BN, ReLU 3×3 Conv, 196 BN, ReLU 2×2 Max-pool	3×3 Conv, 512 BN, LReLU 3×3 Conv, 256 BN, LReLU 3×3 Conv, 128 BN, LReLU Avg-pool
Dense 256→10	Dense 84→10	Dense 256→100	Dense 128→10

B. Additional Experiments

B.1. Approximation to $R(\cdot)$ in Co-teaching

Recall that $R(t)$ in Co-teaching is generated from (1). As all basis functions in Table 1 are smooth, it is not possible for (4) to exactly subsume (1). However, $R(t)$ in (4) can well approximate (1). To illustrate this, we randomly generate three $R(t)$'s in Co-teaching's search space by uniform sampling the corresponding hyperparameters $\tau \in (0, 1)$, $c \in \{0.5, 1, 2\}$ and $t_k \in (0, 200)$. Figure 10 shows the function in (4) that best approximates each of these $R(t)$'s with the least squared error.

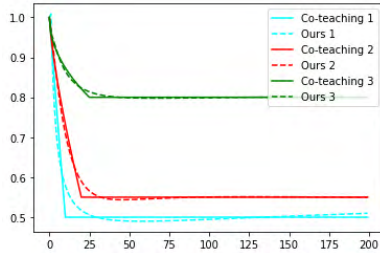


Figure 10. $R(t)$ in Co-teaching and the best approximation from the proposed search space.

B.2. Comparison with Weight Sharing

Weight sharing (Pham et al., 2018; Liu et al., 2019) is a popular method to speed up the search in NAS. In this experiment, we study if weight-sharing is also beneficial to the search of $R(\cdot)$. We compare $S2E$ with $ASNG$ (Akimoto et al., 2019), which is a weight-sharing version of NG. Specifically, $ASNG$ optimizes

$$\min_{\theta, w} \mathcal{G}(\theta, w) \equiv \int_{x \in \mathcal{F}} \mathcal{L}_{\text{val}}(f(w; R(x)), \mathcal{D}_{\text{val}}) p_{\theta}(x) dx,$$

by alternating the updates of w (using gradient descent) and θ (using natural gradient descent). Unlike $S2E$ in (6), in which each θ has its own optimal w^* , $ASNG$ only uses one w that is shared by all θ .

Table 7³ compare the test accuracies of $S2E$ and $ASNG$. As can be seen, the $R(\cdot)$ obtained by $ASNG$ is much worse than that from $S2E$, indicating weight-sharing is not a good choice here. Recently, the problem of weight sharing is also discussed in (Sciuto et al., 2020), which shows that it is not useful in NAS for convolutional and recurrent neural works.

Table 7. Testing accuracies (%) obtained on CIFAR-10 by $ASNG$ and $S2E$.

	sym-20%	sym-50%	pair-45%
$ASNG$	57.82	47.34	41.46
$S2E$	58.73	50.82	47.58

³ it's OK to remove Fig 10, which is just in appendix after all. *** is it really necessary to show Figure ?? i hvnt read the asng paper. but there're 2 disadvantages of showing the fig (1) i suppose what u show in Figure ?? corresponds to the validation acc of the supernet (in wgt sharing). the supernet is not really the network that u use at the end (as u need to perform what u call fine-tuning here). (2) u show the validation acc (that's because it might not make a lot of sense to get back the final net at each step). but w/o a longer explanation, the reader may get confused. but giving a long explanation is a bit off focus √ figure shows validation acc during the search; table reports the final test acc *** if that's just test acc, then there's no need to show the tbl as one can already chk the fig

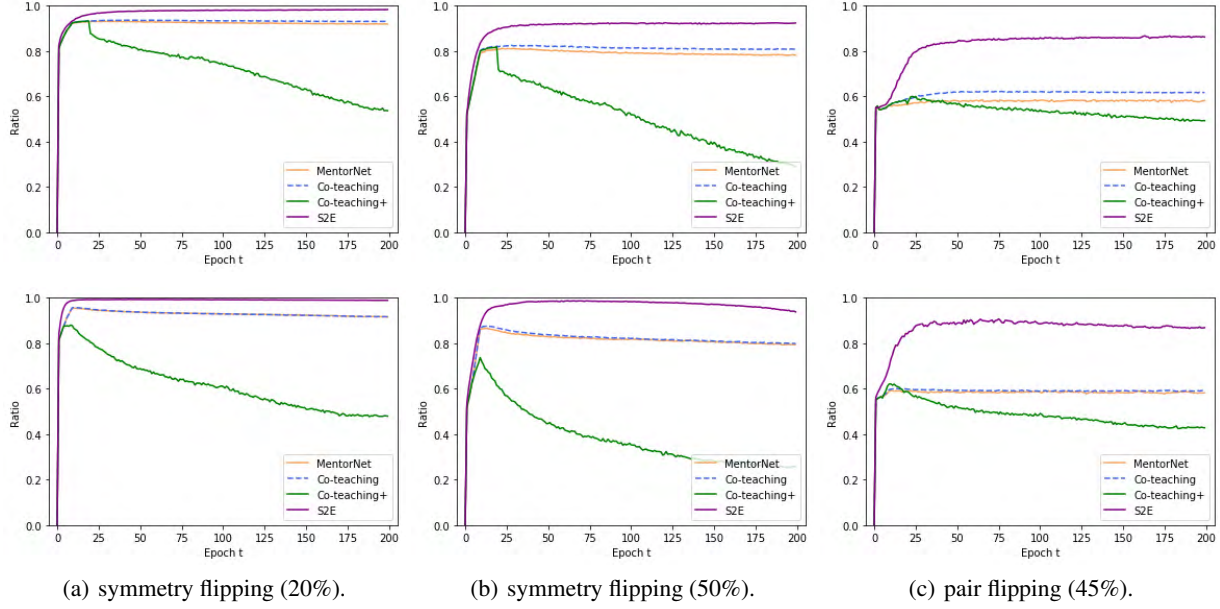


Figure 9. Label precisions of *MentorNet*, *Co-teaching*, *Co-teaching+* and *S2E* on CIFAR-10 (top) and CIFAR-100 (bottom).

C. Proofs

C.1. Proposition 1

Proof. By definition,

$$\begin{aligned}\nabla^2 \mathcal{J}(\theta) &= \int \bar{f}(x) \nabla^2 p_{\theta}(x) dx \\ &= \mathbb{E}_{p_{\theta}} \left[\bar{f}(x) \frac{\nabla^2 p_{\theta}(x)}{p_{\theta}(x)} \right].\end{aligned}\quad (10)$$

Now,

$$\begin{aligned}\nabla^2 \log p_{\theta}(x) &= \nabla \left(\frac{\nabla p_{\theta}(x)}{p_{\theta}(x)} \right) \\ &= \frac{\nabla^2 p_{\theta}(x)}{p_{\theta}(x)} - \frac{\nabla p_{\theta}(x) \nabla p_{\theta}(x)^{\top}}{p_{\theta}^2(x)}.\end{aligned}$$

Thus,

$$\begin{aligned}\frac{\nabla^2 p_{\theta}(x)}{p_{\theta}(x)} &= \nabla^2 \log p_{\theta}(x) + \frac{\nabla p_{\theta}(x) \nabla p_{\theta}(x)^{\top}}{p_{\theta}^2(x)} \\ &= \nabla^2 \log p_{\theta}(x) + \left(\frac{\nabla p_{\theta}(x)}{p_{\theta}(x)} \right) \left(\frac{\nabla p_{\theta}(x)}{p_{\theta}(x)} \right)^{\top} \\ &= \nabla^2 \log p_{\theta}(x) + \bar{p}_{\theta} \bar{p}_{\theta}^{\top},\end{aligned}$$

Result follows on substituting this into (10). \square

C.2. Proposition 2

Proof. First, we introduce the following Lemma 1 which results from Assumption 2.

Lemma 1 ((Rockafellar, 1970)). *Since \mathcal{J} is L -Lipschitz smooth, we have $\mathcal{J}(\mathbf{y}) \leq \mathcal{J}(\mathbf{x}) + \langle \nabla \mathcal{J}(\mathbf{x}), \mathbf{y} - \mathbf{x} \rangle + \frac{L}{2} \|\mathbf{y} - \mathbf{x}\|^2$ for any \mathbf{x} and \mathbf{y} .*

Define a function g as

$$g(\theta; \mathbf{y}, \mathbf{z}, \mathbf{H}) = (\theta - \mathbf{y})^{\top} \mathbf{z} + \frac{1}{2} (\theta - \mathbf{y})^{\top} \mathbf{H} (\theta - \mathbf{y}).$$

Due to (9), we can express θ^{m+1} as

$$\theta^{m+1} = \arg \min_{\theta} g(\theta; \mathbf{y}, \mathbf{z}, \mathbf{H}), \quad (11)$$

where

$$\mathbf{y} = \theta^m, \mathbf{z} = \nabla \mathcal{J}(\theta^m) - \mathbf{e}^m \text{ and } \mathbf{H} = \Delta^m. \quad (12)$$

Note that Δ^m is a positive definite matrix, thus g is a convex function on θ . Consider the directional derivative of g w.r.t. θ at the optimal point $\theta = \theta^{m+1}$, and using the fact that g is a convex function, we have

$$\langle \mathbf{z} + \mathbf{H}(\theta^{m+1} - \mathbf{y}), \mathbf{w}^m \rangle \geq 0 \quad (13)$$

for any direction \mathbf{w} .

Let $\mathbf{w} = \theta^m - \theta^{m+1}$. Combining (12) and (13), we have

$$\langle \nabla \mathcal{J}(\theta^m) - \mathbf{e}^m, \gamma^m \rangle \leq -(\gamma^m)^{\top} \Delta^m \gamma^m. \quad (14)$$

Next, using Lemma 1, we have

$$\begin{aligned}\mathcal{J}(\theta^{m+1}) &\leq \mathcal{J}(\theta^m) + \langle \nabla \mathcal{J}(\theta^m), \theta^{m+1} - \theta^m \rangle \\ &\quad + \frac{L}{2} \|\theta^{m+1} - \theta^m\|^2.\end{aligned}\quad (15)$$

Now, we add the error term e^m in (15), i.e.,

$$\begin{aligned} \mathcal{J}(\theta^{m+1}) &\leq \mathcal{J}(\theta^m) + \langle \nabla \mathcal{J}(\theta^m) - e^m, \theta^{m+1} - \theta^m \rangle \\ &\quad + \frac{L}{2} \|\theta^{m+1} - \theta^m\|^2 + \langle e^m, \theta^{m+1} - \theta^m \rangle, \\ &\leq \mathcal{J}(\theta^m) - (\gamma^m)^\top \Delta^m \gamma^m + \frac{L}{2} \|\theta^{m+1} - \theta^m\|^2 \\ &\quad + \langle e^m, \theta^{m+1} - \theta^m \rangle, \end{aligned} \quad (16)$$

$$\begin{aligned} &= \mathcal{J}(\theta^m) - (\gamma^m)^\top \Delta^m \gamma^m + \frac{L}{2} \|\gamma^m\|^2 + \langle e^m, \gamma^m \rangle, \\ &\leq \mathcal{J}(\theta^m) - (\gamma^m)^\top \Delta^m \gamma^m + \frac{L}{2} \|\gamma^m\|^2 \\ &\quad + \|e^m\|_2 \|\gamma^m\|_2, \end{aligned} \quad (17)$$

$$\begin{aligned} &\leq \mathcal{J}(\theta^m) - \frac{1}{\eta} \|\gamma^m\|^2 + \frac{L}{2} \|\gamma^m\|^2 \\ &\quad + \|e^m\|_2 \|\gamma^m\|_2, \end{aligned} \quad (18)$$

$$= \mathcal{J}(\theta^m) + \frac{\eta L - 2\eta}{2\eta} \|\gamma^m\|^2 + \|e^m\|_2 \|\gamma^m\|_2, \quad (19)$$

where (16) is from (14), (17) is from inequality $\langle \alpha, \beta \rangle \leq \|\alpha\| \|\beta\|$, (18) results from Assumption 3, i.e., the smallest eigen value of Δ^m is not smaller than η . Finally, rearranging terms in (19), we will obtain the Proposition. \square

C.3. Theorem 1

Before proving this Theorem 1, we first introduce the following Lemma 1.

Lemma 2. Define

$$\varepsilon^m = \left\| (\Delta^m)^{-1} e^m \right\| \text{ and } \rho^m = (\Delta^m)^{-1} \mathcal{J}(\theta^m).$$

We have

$$c^m \leq \|\gamma^m\| \leq \|\rho^m\| + \varepsilon^m,$$

where $c^m = \max(\|\rho^m\| - \varepsilon^m, \varepsilon^m - \|\rho^m\|)$.

Proof. Since θ^{m+1} is generated by (9), thus

$$\begin{aligned} \|\gamma^m\| &= \left\| (\Delta^m)^{-1} (\nabla \mathcal{J}(\theta^m) - e^m) \right\|, \\ &= \left\| (\Delta^m)^{-1} e^m + \rho^m \right\|. \end{aligned}$$

Then, the Lemma follows from Cauchy inequality. \square

Now, we start to prove Theorem 1.

Proof of Theorem 1. Since the eigen values of Δ^m are in $[\eta, L]$ (by Assumption 3), we have

$$\frac{1}{L} \|e^m\| \leq \left\| (\Delta^m)^{-1} e^m \right\| \leq \frac{1}{\eta} \|e^m\|. \quad (20)$$

Combining (20) and Proposition 2, we obtain

$$\begin{aligned} \mathcal{J}(\theta^m) - \mathcal{J}(\theta^{m+1}) &\geq \frac{2-L\eta}{2\eta} \|\gamma^m\|^2 - \|e^m\| \|\gamma^m\|, \\ &\geq \frac{2-L\eta}{2\eta} \|\gamma^m\|^2 - \eta(\varepsilon^m)^2 \|\gamma^m\|. \end{aligned} \quad (21)$$

Next, using Lemma 2 in (21), we have

$$\begin{aligned} \mathcal{J}(\theta^m) - \mathcal{J}(\theta^{m+1}) &\geq \frac{2-L\eta}{2\eta} (\|\rho^m\| - \varepsilon^m)^2 \\ &\quad - \eta(\varepsilon^m)^2 (\|\rho^m\| + \varepsilon^m). \end{aligned}$$

Rearranging terms in the above inequality, we have where

$$\begin{aligned} b_1 &= \frac{2-L\eta}{2\eta}, \\ b_2 &= \frac{2-L\eta + \eta^2}{\eta}, \\ \text{and } b_3 &= \frac{2\eta^2 + L\eta - 2}{2\eta}. \end{aligned}$$

First Assertion. Define the following auxiliary function

$$\psi(\theta^m) = b_1 \|\rho^m\|^2 - b_2 \|\rho^m\| \varepsilon - b_3 (\varepsilon^m)^2.$$

With this definition, we have

$$\mathcal{J}(\theta^m) - \mathcal{J}(\theta^{m+1}) \geq \psi(\theta^m). \quad (22)$$

It is easy to see that since $\|\rho^m\|$ and ε are continuous, b_1, b_2 and b_3 are non-negative, then $\psi(\theta^m)$ is lower semi-continuous. Let the sub-level set of ψ be

$$\mathcal{L}(\psi, a) \equiv \{\theta \mid \psi(\theta) \leq a\}, \quad a \geq 0.$$

Note that the sub-level set of $\mathcal{L}(\psi, a)$ is closed for any $a \geq 0$ (see Theorem 7.1 in (Rockafellar, 1970)). Denote $u = \|\rho^m\|$, and resolving the quadratic inequality in u :

$$b_1 u^2 - b_2 \varepsilon^m u - b_3 (\varepsilon^m)^2 - t \leq 0,$$

we conclude

$$u \leq \frac{b_2 \varepsilon^m}{2b_1} + \frac{1}{2b_1} \sqrt{(b_2^2 + 4b_1 b_3)(\varepsilon^m)^2 + 4b_1 a}.$$

Thus,

$$\begin{aligned} \mathcal{L}(\psi, a) &= \{\theta \mid \|\rho^m\| \leq \frac{b_2 \varepsilon^m}{2b_1} \\ &\quad + \frac{1}{2b_1} \sqrt{(b_2^2 + 4b_1 b_3)(\varepsilon^m)^2 + 4b_1 a}\}, \end{aligned}$$

In particular,

$$\mathcal{L}(\psi, 0) = \left\{ \theta \mid \|\rho^m\| \leq \frac{b_2 + \sqrt{(b_2^2 + 4b_1 b_3)}}{2b_1} \varepsilon \right\}.$$

Define

$$d_1 = \frac{b_2 + \sqrt{b_2^2 + 4b_1b_3}}{2b_1} \quad \text{and} \quad d_2 = b_1^{-1}.$$

We conclude

$$\mathcal{L}(\psi, a) \subseteq \left\{ \theta \mid \|\rho^m\| \leq d_1 \varepsilon^m + d_2 a^{\frac{1}{2}} \right\},$$

and

$$\mathcal{L}(\psi, 0) \subseteq \left\{ \theta \mid \|\rho^m\| \leq d_1 \varepsilon^m \right\}. \quad (23)$$

Next, we prove that there exists a limit point $\bar{\theta}$ of $\{\theta^m\}$ such that $\bar{\theta} \in \mathcal{L}(\psi, 0)$. Suppose the opposite holds. By (22), we have

$$\mathcal{J}(\theta^m) - \mathcal{J}(\theta^{m+1}) \geq \psi(\theta^m), \quad \forall m \geq m_1. \quad (24)$$

By Assumption $\lim_{m \rightarrow \infty} \{\theta^m\} \cap \mathcal{L}(\psi, 0) = \emptyset$. Then, since ψ is lower semi-continuous, we have

$$\psi(\theta^m) \geq c > 0,$$

when $m \geq m_2$ for some sufficiently large m_2 and a positive constant c .

Denote $k = \max\{m_1, m_2\}$, for any $m \geq k$, we have

$$\begin{aligned} \mathcal{J}(\theta^k) - \mathcal{J}(\theta^m) &= \sum_{j=m}^k (\mathcal{J}(\theta^j) - \mathcal{J}(\theta^{j+1})), \\ &\geq (k - m)c. \end{aligned}$$

Let $k \rightarrow \infty$, we have $\lim_{m \rightarrow \infty} \mathcal{J}(\theta^m) = -\infty$, which contradicts with Assumption 2, i.e., $\inf \mathcal{J} > -\infty$. Thus, from (23), for every limit point $\bar{\theta}$ of $\{\theta^m\}$, we must have

$$\|\rho^m\| \leq d_1 \varepsilon^m.$$

Recall the definition of ρ^m in Lemma 2, and by Assumption 3 that the error ε^m on gradient is upper-bounded by $\bar{\varepsilon}$, we obtain the first assertion.

Second Assertion. If the sequence $\{\theta^m\}$ converges, then for every sub-sequence $\{\theta^{m_i}\}$ of $\{\theta^m\}$ it follows

$$\lim_{i \rightarrow \infty} \sup \mathcal{J}(\theta^{m_i}) = \lim_{m \rightarrow \infty} \inf \mathcal{J}(\theta^m),$$

Thus,

$$\lim_{m \rightarrow \infty} \theta^m \subseteq \mathcal{L}(\psi, 0), \quad (25)$$

where $\mathcal{L}(\psi, 0)$ is in (23). Combing (25) with the first assertion, we then have

$$\lim_{m \rightarrow \infty} \|\varepsilon^m\| \leq c_1 \bar{\varepsilon}.$$

Finally, by (i) in Assumption 2 and definition of ε^m in Lemma 2, we have

$$\lim_{m \rightarrow \infty} \|e^m\| \leq c_2 \bar{\varepsilon},$$

for a positive constant c_2 , which proves the second assertion. \square